



HAL
open science

Annealing of thin Zr films on Si_{1-x}Gex ($0 \leq x \leq 1$): X-ray diffraction and Raman studies

Odette Chaix-Pluchery, Bernard Chenevier, Valérie Aubry-Fortuna, Igor Matko

► **To cite this version:**

Odette Chaix-Pluchery, Bernard Chenevier, Valérie Aubry-Fortuna, Igor Matko. Annealing of thin Zr films on Si_{1-x}Gex ($0 \leq x \leq 1$): X-ray diffraction and Raman studies. *Journal of Physics and Chemistry of Solids*, 2002, 63, pp.1889. hal-00207762

HAL Id: hal-00207762

<https://hal.science/hal-00207762>

Submitted on 18 Jan 2008

HAL is a multi-disciplinary open access archive for the deposit and dissemination of scientific research documents, whether they are published or not. The documents may come from teaching and research institutions in France or abroad, or from public or private research centers.

L'archive ouverte pluridisciplinaire **HAL**, est destinée au dépôt et à la diffusion de documents scientifiques de niveau recherche, publiés ou non, émanant des établissements d'enseignement et de recherche français ou étrangers, des laboratoires publics ou privés.

Annealing of thin Zr films on $\text{Si}_{1-x}\text{Ge}_x$ ($0 \leq x \leq 1$) :

X-ray diffraction and Raman studies

O. CHAIX-PLUCHERY^{a,*}, B. CHENEVIER^a, V. AUBRY-FORTUNA^b, I. MATKO^a

^a Laboratoire des Matériaux et du Génie Physique (CNRS UMR 5628), ENSPG-INPG, BP 46, 38402 St Martin d'Hères Cedex, France

^b Institut d'Electronique Fondamentale (CNRS UMR 8622), Bât. 220, Université Paris Sud, 91405 Orsay Cedex, France

* Corresponding author; e-mail address: Odette.Chaix@ inpg.fr

Abstract: X-ray diffraction experiments have been combined to Raman scattering and transmission electron microscopy data to analyze the result of rapid thermal annealing applied to Zr films, 16 or 80 nm thick, sputtered on $\text{Si}_{1-x}\text{Ge}_x$ epilayers ($0 \leq x \leq 1$). The C49 $\text{Zr}(\text{Si}_{1-x}\text{Ge}_x)_2$ is the unique phase obtained after complete reaction. $\text{ZrSi}_{1-x}\text{Ge}_x$ is formed as intermediate phase. The C49 formation temperature T_f is lowered by the addition of Ge in the structure. Above a critical Ge composition close to $x=0.33$, a film microstructure change was observed. Films annealed at temperatures close to T_f are continuous and relaxed. Annealing at $T > T_f$ leads to discontinuous films: surface roughening resulting from SiGe diffusion at film grain boundaries occurred. Grains are ultimately partially embedded in a SiGe matrix. A reduction in the lattice parameters as well as a shift of Raman lines are observed as T exceeds T_f . Both Ge non-stoichiometry and residual stress have been considered as possible origins of these changes. However, as Ge segregation has never been detected, even by using very efficient techniques, it is thought that the changes originate merely from residual stress. The C49 grains are expected to be strained under the SiGe matrix effect and the shift of the Raman lines would indicate the stress is compressive. Some simple evaluations of the stress values indicate that it varies between -0.3 and -3.5 GPa for $0 \leq x \leq 1$ which corresponds to a strain in the range [-0.11, -1.15 %]. X-ray and Raman determinations are in good agreement.

Keywords : Zr/SiGe thin films, Raman spectroscopy, X-ray diffraction, elastic properties, microstructure.

1. Introduction

The potential technological applications of transition metal germanosilicides in microelectronic devices as metallic contacts with SiGe alloys are subjects of many investigations. Their formation by metal-SiGe solid state reaction and stability as thin films are specifically studied.

In the Zr-SiGe system, the thermally induced solid phase reaction in Ge concentration ranges limited to $\text{Si}_{0.5}\text{Ge}_{0.5}$ has been the subject of recent studies in spite of the rather high resistivity of the zirconium germanosilicide in comparison with others such as the C54 phase of $\text{Ti}(\text{SiGe})_2$. ZrSi_2 and ZrGe_2 have the C49 orthorhombic stable crystal structure with very similar lattice parameters. Studies of the structural properties and stability of the germanosilicide formed by solid state reaction of Zr with $\text{Si}_{1-x}\text{Ge}_x$ [1] reveal that Zr reacts uniformly with $\text{Si}_{1-x}\text{Ge}_x$ and that C49 $\text{Zr}(\text{Si}_{1-y}\text{Ge}_y)_2$ with $y=x$ is the final phase. $\text{Zr}(\text{Si}_{1-x}\text{Ge}_x)$ is found to be an intermediate phase prior to the formation of the C49 phase. Another study indicates Zr_4Ge_5 as an intermediate compound in the $\text{Zr}/\text{Si}_{0.5}\text{Ge}_{0.5}$ system [2]. The $\text{Zr}(\text{Si}_{1-x}\text{Ge}_x)_2$ films formed by annealing at 700°C are continuous films consisting of grains which islanded for long annealings. No Ge segregation is detected. The sheet resistance of the C49 $\text{Zr}(\text{Si}_{1-x}\text{Ge}_x)_2$ films is found to be higher than that of C49 ZrSi_2 [1].

As Ge segregation upon annealing can be very detrimental to device performance, it has been thoroughly studied in several M-SiGe systems. Differences of Ge content between $\text{Si}_{1-x}\text{Ge}_x$ alloy and germanosilicide films have been detected in systems where $M = \text{Co}$ [3], W [4], Pd , Ni , Pt , Ti (see [5] and references therein). Ge segregation is stronger in the Co and W -SiGe systems. In the case of Co , it is explained by the non-miscible character of CoGe_2 in CoSi_2 . For a W contact, W -Ge compounds are not easy to form, except at high temperatures and under high pressures. Therefore, W reacts to form WSi_2 only and Ge is rejected at the interface [4]. In the case of Ti , the Ge composition y of the final C54 $\text{Ti}(\text{Si}_{1-y}\text{Ge}_y)_2$ is always lower than x in the initial $\text{Si}_{1-x}\text{Ge}_x$ alloy. The excess Ge diffuses into the C54 grain boundaries where it combines with the $\text{Si}_{1-x}\text{Ge}_x$ substrate and precipitates as $\text{Si}_{1-z}\text{Ge}_z$ ($z>x$) [2, 3, 6-8]. In addition to the compound formation, a strain relaxation of the unreacted SiGe epilayer is reported, which can be important as soon as Ge segregates. In the Zr-SiGe system, the absence of Ge segregation during the Zr germanosilicide formation is usually explained by a reduced mobility of Si and Ge compared with the C54 $\text{Ti}(\text{Si}_{1-y}\text{Ge}_y)_2$ and by a lower thermodynamic driving force for Ge segregation in the Zr-SiGe system than in the Ti-SiGe system. Other studies concerning the electrical properties and thermal stability of the Zr phases formed in the $\text{Zr-Si}_{1-x-y}\text{Ge}_x\text{C}_y$ system after rapid thermal annealing have been reported [9-10]. Similar phase sequences have been obtained upon annealing, with C49 $\text{Zr}(\text{Si}_{1-x}\text{Ge}_x)_2$ as the final phase of the reaction at 800°C . The presence of C does not modify the reaction but it prevents strain relaxation [11].

In this work, we have investigated the $\text{Zr}/\text{Si}_{1-x}\text{Ge}_x$ film solid state reaction in Ge concentration ranges extended to $x=1$ ($0 \leq x \leq 1$) as a function of the annealing temperature and metal thickness. The present paper is mainly devoted to the film microstructure analysis performed by using X-ray

diffraction and to Raman scattering results. A previous paper [5] reports on phase identification and surface morphology results. To our knowledge, the whole ZrSi_2 Raman spectrum has never been reported because of the low intensity and rather complex Raman spectra of ZrSi_2 films and of the lack of single crystals. We have also performed the $\text{Zr}(\text{Si}_{1-x}\text{Ge}_x)_2$ Raman spectrum analysis in the whole Ge composition range. A lot of results have been obtained. Specific effort has been made for the understanding of the thinnest film behavior. Additionally, Transmission Electron Microscopy observations have been performed to help understanding of the film behavior at the highest temperatures.

2. Crystal structure and Raman modes

2.1. Crystal structure

ZrSi_2 and ZrGe_2 crystallize in the C49 base centered orthorhombic structure (space group Cmc_m or D_{2h}^{17}) with four formula units per unit cell. The lattice constants are $a=0.36958$ nm, $b=1.4751$ nm, $c=0.36654$ nm for ZrSi_2 [JCPDS 32-1499], $a=0.3789$ nm, $b=1.4975$ nm, $c=0.3761$ nm for ZrGe_2 [JCPDS 72-1200]. ZrSi and ZrGe also crystallize in the orthorhombic structure with four formula units per unit cell (space group Pnma). The ZrSi lattice constants are $a=0.6981$ nm, $b=0.3785$ nm, $c=0.5301$ nm [JCPDS 9-226].

The primitive cell of the C49 crystal structure contains two ZrSi_2 molecules. Illustrations of the structure are given in references [12-13]. The silicon atoms are distributed into two Si(I) and two Si(II) inequivalent sites. Si(I) atoms are contained in (010) planes independently of other atoms; Si(II) atoms are close to the Zr planes. Each Zr atom has ten near-neighbor Si atoms at distances in the range 0.270-0.295 nm : four nearest-neighbor Si(II) and six more distant Si neighbors (4 Si(I) + 2 Si(II)). Each Si atom has eight near-neighbors : four Zr and four Si(I) around Si(I), six Zr and two Si(II) around Si(II).

2.2. Vibrations in ZrSi_2

The metal and silicon atoms are in special position 4c with site symmetry mm (or C_{2v}). The six atoms of the primitive unit cell give rise to 18 zone center vibrational modes. Using group-theory calculations and specially the correlation method as reviewed by Fateley [14], we can identify the irreducible representations associated with the vibrational modes after subtraction of the three acoustic modes ($B_{1u} + B_{2u} + B_{3u}$) :

$$\Gamma_{\text{vib}} = 3A_g + 3B_{2g} + 3B_{3g} + 2B_{1u} + 2B_{2u} + 2B_{3u}$$

where A_g, B_{2g}, B_{3g} are Raman-active modes and B_{1u}, B_{2u}, B_{3u} are IR-active modes. Thus, nine Raman lines, relative to nine non degenerate modes, are expected in the ZrSi_2 and $\text{Zr}(\text{Si}_{1-x}\text{Ge}_x)_2$ spectra.

3. Experimental details

3.1. Samples

$\text{Si}_{1-x}\text{Ge}_x$ layers ($0 \leq x \leq 1$) of 0.1 to few μm of thickness were epitaxially grown by Rapid Thermal Chemical Vapor Deposition [15-18] or Molecular Beam Epitaxy [19] on (100) Si substrate, at temperatures ranging from 550 to 800°C. The $\text{Si}_{1-x}\text{Ge}_x$ layers were either pseudomorphic ($x \leq 0.13$), or relaxed ($x \geq 0.17$). Some of the relaxed $\text{Si}_{1-x}\text{Ge}_x$ layers were grown on top of a relaxed graded composition $\text{Si}_{1-m}\text{Ge}_m$ layer (m from 0 to x). Prior to metal deposition, each SiGe sample surface was cleaned by using a standard chemical procedure, followed by a dip in dilute HF and a final rinsing in deionized water. 16, 80 and 200 nm thick Zr films were deposited at room temperature in a dc magnetron sputtering chamber using low cathode voltage (70 V). Heat treatments were performed in a Rapid Thermal Annealing (RTA) system under Ar/ H_2 atmosphere. The annealing temperatures T were varying from 385 to 920°C for 5 min.

3.2. X-ray diffraction

The various phases formed during annealing were analyzed by X-ray diffraction at room temperature using a Siemens D500 $\theta/2\theta$ diffractometer ($\lambda_{\text{Cu}_{K\alpha 1}} = 0.15406$ nm). The rocking curves of the strongest X-ray lines of some films were measured using a Siemens D500 diffractometer ($\lambda_{\text{Fe}_{K\alpha}} = 0.1936$ nm). This was done to estimate the degree of orientation of the films (or of alignment of the grains).

3.3. Raman scattering

Raman spectra were collected using a Dilor XY multichannel spectrometer and a CCD detector. Experiments were conducted in micro-Raman mode at room temperature in a backscattering geometry. The 514.5 nm line of an Ar^+ ion laser was focused to a spot size smaller than 1 μm^2 . The incident laser power, measured at the surface of the sample, was between 1.5 and 3 mW in order to be much lower than the heating threshold of the samples and thus, to prevent any excessive sample heating able to alter the film microstructure. As expected from metal compounds, the Raman signal was weak and 30 min acquisition times were necessary. The instrumental resolution was 2.8 ± 0.2 cm^{-1} .

As $\text{Zr}(\text{Si}_{1-x}\text{Ge}_x)_2$ Raman lines were very weak, it was clearly not possible to record Raman spectra using a setting able to perform a full polarization analysis. To obtain polarized Raman spectra, we varied only the incident beam polarization direction.

3.4. Transmission electron microscopy

Cross-section TEM observations have been performed by using a JEOL 200CX microscope.

4. X-ray diffraction results

The solid state reaction between Zr and the underlying $\text{Si}_{1-x}\text{Ge}_x$ alloy has been investigated in the whole Ge composition range $x=0-1$, the two extreme substrates being (100) Si and (100) Ge. Whereas the diffraction signal from textured as-deposited Zr films is very strong, the line intensities from annealed films are very difficult to record with satisfactory statistics. However, a sufficient number of characteristic reflections have been collected to identify the phases at each reaction stage. In addition, some multiple diffraction contributions of substrates are also noticed in the X-ray diagrams. Two main effects of film annealing revealed by X-ray diffraction will be pointed out: one is relative to the reaction itself, the second one to the film microstructure.

4.1. Crystal phase identification as a function of annealing

The typical X-ray pattern of a 16 nm-thick Zr film deposited on $\text{Si}_{1-x}\text{Ge}_x$ is given in Fig. 1 as a function of the annealing temperature in the case of $x=0.33$. The low film thickness and the weak scattering power of the elements resulted in weak diffracted intensities. Special care has therefore been required to obtain unambiguous phase identification.

The as-deposited films consist of hexagonal Zr (S.G. $P6_3/mmc$). Texture changes from pure 002 in 16-80 nm-thick Zr films to mixed 002 and 100 components as film thickness increases.

Upon heating, several steps can be distinguished. First, at temperature lower than 400°C , the Zr film recrystallizes and the diffraction pattern characteristic of a 002 texture component changes to a powder-like pattern in which weak Zr and ZrSiGe reflections coexist (see Fig. 1b). This indicates that the film-epilayer reaction has started. As the temperature is further raised, SiGe incorporation progresses (see Fig. 1c, 1d). At $T=790^\circ\text{C}$ (Fig. 1e), the reaction is complete: the film has the C49 $\text{Zr}(\text{Si}_{1-x}\text{Ge}_x)_2$ structure. The temperature required to transform the whole Zr film into the unique C49 final phase will be designated by T_f in the following ($T_f = 790^\circ\text{C}$ in the present case, Fig. 1e), and the annealing temperatures higher than T_f by T_a . Films annealed at T_a give systematically less intense reflections shifted towards higher 2θ angles (Fig. 1f) although the final phase is always the C49 phase.

4.2. C49 line profile evolution

Further investigations of the profiles of the three main C49 X-ray lines (060, 131 and 002) have been carried out to study the film microstructure as a function of Ge incorporation ($0 \leq x \leq 1$).

As the Ge rate progressively increases, the variation of the angular positions of the C49 phase diffraction lines indicates that Ge is incorporated in the structure. As T is close to T_f , a plot of the d-spacings as a function of the Ge-content nearly follows a Vegard's law defined from ZrSi_2 and ZrGe_2 bulk data (Fig. 2). However, annealing temperatures higher than T_f lead to $d(x)$ much lower than the values expected from the Vegard's law (Fig. 2). A greater d-spacing reduction is observed for the (131) planes.

Fig. 3a reports normalized $\theta/2\theta$ scans of the C49 lines obtained from 16 nm Zr films annealed at T_f as a function of x . For $x < 0.33$, the intensities are typical of a powder diagram. For x close to 0.33, the 131 and 060 line intensities are nearly equal to each other, which means that a preferred orientation of the film is being settled, as for a powder sample the ratio I_{060}/I_{131} should be close to 16/100. This effect is progressively amplified as x increases. Above $x=0.33$, the 060 line intensity increases abruptly up to $x=1$.

Rocking curve measurements in a series of annealed films with $0.33 \leq x \leq 0.71$ (16 nm Zr, $710^\circ\text{C} \leq T \leq 820^\circ\text{C}$) indicate that the intensity increase is brought about by the development of a 060 texture component (see Table 1). The evolution of the 060 $\theta/2\theta$ scans and of the corresponding rocking curve in this temperature range are shown in Fig. 4 for $x=0.38$ but this temperature behavior can be extended to other Ge-contents reported in Table 1. T_f is close to or slightly lower than 800°C . A linewidth decrease occurs in the $\theta/2\theta$ scan when increasing T from 710° to 800°C whereas the integrated intensity remains rather constant. After annealing at 820°C , both a line intensity decrease and a lineshift are observed (Fig. 4a). The corresponding rocking curves show that the 060 texture remains rather stable up to 800°C (half width at half maximum (HWHM) close to 3° , see Table 1) whereas grain alignment is improved above this temperature (HWHM close to 1° for $T=820^\circ\text{C}$) (Fig. 4b). Note that the intensities of a reflection in the $\theta/2\theta$ and ω -scans are correlated.

Unlike thinner films, the relative intensities do not depend upon x in 80 nm Zr films for low x values (Fig. 3b). No thick film was available on substrate with $x > 0.33$. Rocking curves measured on such films deposited on $\text{Si}_{0.67}\text{Ge}_{0.33}$ and annealed at 800°C are characteristic of a powder-type microstructure. So, the 060 texture observed in thin films for $x=0.33$ is progressively suppressed as films become thicker.

The C49 ZrSi_2 diffraction pattern reveals lines two to three times broader than the instrumental width (FWHM close to 0.12 and $0.15^\circ 2\theta$ for λ_{Cu} and λ_{Fe} , respectively) for both 16 and 80 nm film thicknesses. The corresponding powder grain size, calculated using the classical Scherrer formula, varies between 34 and 40 nm. No clear x dependence of the linewidths could be detected.

4.3. Influence of the Ge-content on the formation temperature of the silicide phases

Two main points can be emphasized:

- (i) the formation temperature of the C49 phase obtained with 16 nm thick Zr films is lowered with Ge incorporation: T_f is roughly linearly decreasing with increasing x , from 810°C ($x=0$) to 720°C ($x=1$) in spite of some noticeable decreasing jump for $0.38 \leq x \leq 0.47$ (see Fig. 2 in [5]). A similar observation is reported for the $\text{Ti-Si}_{1-x}\text{Ge}_x$ system [20].
- (ii) T_f is also lowered by increasing the Zr film thickness independently of the Ge effect, from 810°C to 780°C when passing from 16 to 200 nm Zr ($x=0$). This effect is well-known in Ti films and ascribed to an increase of the surface to volume ratio of the C54 TiSi_2 nucleus when decreasing the film thickness [6].

From an accurate measurement of the 004 SiGe 2θ X-ray line position, it is usually possible to determine the Ge-content of the $\text{Si}_{1-x}\text{Ge}_x$ alloy by assuming a Vegard's law is followed. By using this method, we have shown that the Ge concentration in the alloy is not significantly altered by thermal annealing, in the whole range of Ge composition ($0 \leq x \leq 1$) and whatever the film thickness. This behavior differs from that of annealed Ti films from which Ge-enriched SiGe areas coexisting with Ti germanosilicide film have been detected [5-6]. The Ge segregation gives rise to additional 004 SiGe lines whose angular positions depend on x (see Fig. 4 in [5]).

5. Raman scattering results

Most of the silicide and germanosilicide Raman lines have low intensity. In the Zr case, the Raman spectrum is complex and the lines, numbered 1-9 in the following, had to be fitted using lorentzian profiles, with a particular care paid for spectra recorded from films with high x values because line intensities are very weak. In such cases where profiles were difficult to resolve, constraints have been applied on the linewidths. The multiple bands centered around 215 and 260 cm^{-1} have been decomposed into three (lines 2-4) and two (lines 5-6) individual lorentzian components, respectively. In the 240-350 cm^{-1} region, three groups of $\text{Zr}(\text{SiGe})_2$ lines exist in addition to the Ge-Ge line. The Ge-Ge line was to some extent superimposed either to line 7 for low x values, or to line 8 for $x \geq 0.33$. As Ge-Ge line has very low intensity, it was specifically difficult to resolve from multi-component profiles. No Raman line has been observed neither from the Zr film nor from the $\text{Zr}(\text{SiGe})$ phase. The lines pointed in any spectrum at and below 140 cm^{-1} are due to air.

The ZrSi_2 Raman spectrum related to a 16 nm thick Zr film annealed at 810°C will be presented first. The lines cannot be assigned because single crystal data are missing. The low film thickness allows the Si substrate line to be observed at 520.6 cm^{-1} . A similar spectrum is measured from a thicker ZrSi_2 film (80 nm Zr). The Si line is not observed because the laser beam is absorbed in the thick ZrSi_2 film. The low ZrSi_2 film thickness, close to 35 nm ($=16 \times 2.2$; the expansion factor value = 2.2 has been calculated on the basis of Zr and ZrSi_2 bulk densities) is then close to the penetration depth of the laser beam in ZrSi_2 . The next sections will be devoted to the influence of Ge-content and annealing temperature on the Raman spectrum. The whole Raman results presented later are relative to thin films (16 nm Zr deposits) previously analyzed by X-ray diffraction.

5.1. ZrSi_2

As expected from the Raman mode analysis in Section 2.2, the Raman spectrum recorded from a Zr/Si film annealed at 810°C consists of nine lines in the range 152-333 cm^{-1} (Fig. 5). Lines at 152, 288, 323.7, 332.5 cm^{-1} (lines 1, 7-9) are well defined. Lines obtained after deconvolution have been pointed at 258.8 and 265.7 cm^{-1} (lines 5-6) for the 260 cm^{-1} multiple band and at 204, 211 and 218.6

cm^{-1} (lines 2-4) for the 215 cm^{-1} band. In the last case, the line at 218.6 cm^{-1} is well defined while both other lines are very weak.

5.2. $\text{Zr}(\text{Si}_{1-x}\text{Ge}_x)_2$

For low x values ($x \leq 0.17$), Raman spectra are very similar to the ZrSi_2 one. Lines are nevertheless slightly shifted towards low wavenumbers when increasing x . This comes from the mass effect of the Ge atoms. The Raman line observed above 500 cm^{-1} is assigned to the Si-Si vibrational mode of the SiGe alloy. Note it is abnormally intense in the $x=0.17$ spectrum. The reaction was not complete in this film ($T=775^\circ\text{C}$, i.e. $T < T_f$): a $\text{ZrSi}_{1-x}\text{Ge}_x + \text{Zr}(\text{Si}_{1-x}\text{Ge}_x)_2$ mixture has been identified by X-ray diffraction. Therefore, the film thickness was probably thinner than 35 nm which allows the laser beam penetration into the SiGe layer. The Si-Ge (about 400 and 432 cm^{-1}) and Ge-Ge (about 285 cm^{-1}) Raman lines begin to be noticeable in the spectrum when $x=0.17$. From $x=0.33$, the $\text{Zr}(\text{Si}_{1-x}\text{Ge}_x)_2$ line intensities slowly decrease with increasing x , except the multiple band centered around 215 cm^{-1} . The ZrGe_2 spectrum is composed of a multiple band centered around 180 cm^{-1} and weak lines at 228 , 255 and 320 cm^{-1} ; the Ge substrate line is observed at 300 cm^{-1} . Although ZrSi_2 and ZrGe_2 have the same crystal structure, their Raman spectra are different and the ZrSi_2 Raman lines are better defined.

By taking ZrSi_2 as reference, seven over the nine lines are shown to be linearly shifted towards lower wavenumbers as x increases. The two other lines are only observed for low x values (Fig. 6). The Ge-Ge line shifts slowly towards higher wavenumbers (see Fig. 5): it was pointed at 286.4 , 287.5 and 300.4 cm^{-1} for $x=0.33$, 0.47 and 1 , respectively. In this range, it is superimposed either to line 7 or to line 8.

The $\text{Zr}(\text{Si}_{1-x}\text{Ge}_x)_2$ Raman line intensities are nearly insensitive to modifications of incident beam polarisation. There is no significant in-plane grain alignment in Zr germanosilicide films.

5.3. Influence of annealing

The thermal evolution of Raman spectra of annealed films is the same whatever x in the range 0.33 - 0.71 (Fig. 7) and will be discussed for $x=0.47$ (Fig. 7c). First, intense $\text{Si}_{1-x}\text{Ge}_x$ lines are observed in the as-deposited film. Their intensity is maintained stable up to a temperature from which the solid state reaction starts. Then, the intensities decrease as the temperature increases and the reaction progresses (605 - 715°C). For $715^\circ\text{C} \leq T \leq 815^\circ\text{C}$, i.e. on both sides of the T_f temperature (not well-defined for $0.38 \leq x \leq 0.47$ as mentioned above), the spectrum is composed of rather weak SiGe and $\text{Zr}(\text{Si}_{1-x}\text{Ge}_x)_2$ lines, excepted the lines at 215 cm^{-1} which are more intense. For higher annealing temperatures, the SiGe lines grow again as temperature increases, up to their initial intensities in the as-deposited film are attained, as seen for $T_a=920^\circ\text{C}$. Therefore, the annealing temperature dependence of the SiGe line intensity allows us to estimate T_f for each x value. So, T_f is expected to be close to 800°C for $x=0.38$ (Fig. 7b). In films with $x=0.33$ (Fig. 7a) and $x=0.71$ (Fig. 7d), T_f is either slightly lower or slightly higher than 790°C and 710°C , respectively. Concerning the $\text{Zr}(\text{Si}_{1-x}\text{Ge}_x)_2$ lines observed at

about 215 cm^{-1} , they are shifted towards higher wavenumbers with increasing the temperature above T_f whatever x .

6. TEM results

A TEM cross-section image of a C49 film (16 nm Zr, $x=0.71$, $T=815^\circ\text{C}$) is shown in Fig. 8. Dark stripes in grains 1- 4 of Fig. 8 are characteristic of the C49 phase [21-23]. They result from stacking along the b direction of structural blocks separated by stacking faults. The stripe orientation gives unambiguously the crystal [010] direction. In the grains labelled 1 - 4, the stacking faults are 120° oriented from each other. The determination of grain boundary planes and their structural analysis will be reported in a forthcoming paper. The important results of concern here are :

- Annealing at $T>T_f$ induces recrystallization and thus, specific orientation relationship. In particular, [010] oriented grains represent a minor fraction of grain population.
- The grain thickness is also considerably scattered from 25 nm to more than 65 nm. A single grain with (010) planes parallel to the free surface is observed in the image.
- The film is no longer continuous. $\text{Si}_{1-x}\text{Ge}_x$ blocks are clearly identified. Surface diffusion is not restricted to these blocks. It can extend and cap the C49 film. This ultimately results in embedded C49 grains in a $\text{Si}_{1-x}\text{Ge}_x$ matrix.

7. Discussion

Analysis of the wealth of results reported above allows to infer a series of characteristic structural features as function of annealing temperature. A summary of the analysis is provided in the following. It has to be noted that our conclusions are in very good agreement with those reported by Wang for $x\leq 0.5$ [1]:

- the unique C49 $\text{Zr}(\text{Si}_{1-x}\text{Ge}_x)_2$ final phase is obtained whatever the Ge-content of the substrate ($0\leq x\leq 1$) and the film thickness. The C49 film is continuous, as shown by sheet resistance, RBS and TEM measurements [5]. The as-deposited Zr thin film, 16 - 80 nm of thickness, is found to have a [0001] preferred orientation. The intermediate phase prior to the C49 formation is always found to be $\text{ZrSi}_{1-x}\text{Ge}_x$.
- the Ge-content of the C49 phase is the same as in the underlying $\text{Si}_{1-x}\text{Ge}_x$ alloy, as indicated by the C49 lattice parameter expansion with increasing x following a Vegard's law. The germanosilicide film is then stress-free and the corresponding lattice parameters $d(T_p)$ are defined accordingly as stress-free lattice parameters (Fig. 2, $T=T_p$).

- the C49 formation temperature T_f is lowered as Ge is incorporated in the structure. The same observation in the Ti-Si_{1-x}Ge_x system is explained by a decrease of the C49 to C54 nucleation barrier [6]. In the Zr case, it can be due to a decrease of the ZrSi_{1-x}Ge_x to C49 Zr(Si_{1-x}Ge_x)₂ nucleation barrier.

The film microstructure analysis and Raman spectra evolution indicate that there exists a critical Ge composition close to $x=0.33$ in thin Zr(Si_{1-x}Ge_x)₂ films (16 nm Zr). The C49 film microstructure is of powder-type for low Ge-contents while a 060 texture appears as soon as $x \geq 0.33$. The 060 line intensity increases with increasing x . Raman spectra of C49 films with $x < 0.33$, composed of nine lines, are very similar to each other, i.e. to that of ZrSi₂. Some lines vanish when $x \geq 0.33$; the remaining lines have weak intensities except those at roughly around 215 cm⁻¹. A polarisation analysis shows no noticeable polarisation effect in the Raman spectra as x increases.

A simple solid solution effect could explain the intensity reduction in the Zr(Si_{1-x}Ge_x)₂ Raman spectrum as a function of x . Due to the large atomic size of Ge atoms compared to Si atoms (Ge : 0.122 nm, Si : 0.111 nm), the vibration modes involving only Si motions in ZrSi₂ should be the most attenuated modes as Ge concentration increases. The vibration modes where metal atoms contribute should be less affected. As usually low wavenumber modes are metal dependent [24] and as the modes we observed are Si/Ge dependent, we expected the modes associated with the 215 cm⁻¹ involve Si/Ge and metal motions. Additionally, the Raman shift evolution of the main line (218.6 cm⁻¹) of the 215 cm⁻¹ group approximately follows a $M_{Zr}^{-1/2}(Si_{1-x}Ge_x)_2$ law. However, a departure from the mass law, increasingly important with x , is detected. This probably implies that a refined mass model should be used. The use of a simulation program is considered to go further in the interpretation of the Raman spectrum evolution as x increases. It would allow the line assignment and then, the location of the Ge atoms on both possible Si sites. Among both possible sites, Si(I) sites seem to be the most favourable sites to Ge substitution because they belong to rather independent (010) planes and they have greater interatomic distances.

As annealing temperatures exceed T_f , changes occur in the X-ray diffraction patterns and in the Raman spectra. The drastic increase of the SiGe Raman line amplitude at the expense of most of the C49 Raman lines gives evidence of SiGe diffusion from the SiGe-C49 interface up to the film free surface. Additional confirmation of diffusion has also been obtained from our RBS, SEM and transport property measurements that indicated the formation of a discontinuous Zr(Si_{1-x}Ge_x)₂ film and the presence of SiGe at the film surface [5]. The cross-section TEM image of Fig. 8 provides further information. From the dark stripe orientations characteristic of extended planar defects perpendicular to [010], the orientation relationship between adjoining grains could be determined but will not be discussed here. The proportion of 060 oriented crystals is clearly not overwhelming. This leads to the intensity reduction occurring as $T > T_f$.

The decrease of the d-spacings as well as the shift towards higher wavenumbers of the 215 cm⁻¹ Raman multiple line can be understood in terms of either Ge non-stoichiometry of the C49 film or residual stress. However, Ge segregation has never been detected in annealed Zr films [1, 5].

Moreover, the comparison of the X-ray diagrams of annealed Ti and Zr films indicate that additional 004 SiGe lines relative to Ge-enriched alloy areas due to Ge segregation only occur in the case of Ti [5]. The d-spacing reduction as well as the shift of the Raman line observed as $T > T_f$ would lead to excessive variation of Ge content in the film. For $x=0.71$ and T varying between 710 and 815°C, $\Delta d_{060} = -0.023 \text{ \AA}$ and $\Delta d_{131} = -0.029 \text{ \AA}$ which would correspond approximately to a Ge content $y=0.30$. Similarly, the Raman shift $\Delta\Omega = 8 \text{ cm}^{-1}$ would give $y=0.38$. It is very unlikely that such a great loss of Ge is not correlated with Ge segregation. Accordingly, we have considered these important changes due to residual stress. In such a case, the C49 grains would be strained under the SiGe matrix effect when $T > T_f$ and the shift towards higher wavenumbers of the 215 cm^{-1} Raman line would be characteristic of a compressive stress. The TEM image leads us to think that the grain embedding can cause a hydrostatic compressive stress on the grains and, therefore, an isotropic decrease of the lattice parameters. Indeed, the decrease of the d-spacings is observed along the surface normal, whatever the grain orientation and, therefore, whatever the considered planes. As a consequence of hydrostatic stress, d-spacings in the perpendicular direction must also be reduced. An analysis of the lattice parameters in a direction parallel to the interface has been considered but the weakness of the off-normal reflections prevented us to carry out the measurements.

The detailed analysis of stresses in grains using the inclusion method of Eshelby [25-28] is not developed here. Nevertheless, the Raman shift amplitude $\Delta\Omega$ and the variation of the d-spacing values along the surface normal when increasing $T > T_f$ allow us to give an approximate stress value. In the first stage, we will discuss stress set-up in the germanosilicide film for a particular Ge-content ($x=0.71$). The discussion will then be extended to the whole composition range.

For $x=0.71$, $\Delta\Omega = 8 \text{ cm}^{-1}$ when T is varying from 710°C to 815°C. Using a Raman conversion factor of $3 \text{ cm}^{-1}/\text{GPa}$ [29], the corresponding stress σ should be close to -2.6 GPa. To obtain strain values for the C49 film, Young's modulus ($E = 142 \text{ GPa}$) and Poisson's ratio ($\nu=0.27$) of C49 TiSi_2 [30] have been incorporated in the expression $\epsilon_R = \frac{(1-2\nu)\sigma}{E}$. ϵ_R is found close to -0.8%. The average strain value ϵ_{RX} obtained from the d-spacing variation is -0.9%. As calculations have been done within large approximations, both stress determinations are in reasonably good agreement.

Attempts to understand the possible origin of the compressive stress have been made from the use of simple elastic model. For a solid state reaction at high temperature, the stress measured at room temperature σ is the result of intrinsic σ_{int} and extrinsic σ_{ext} stress components: σ_{int} is due to the lattice mismatch between the grains and the matrix, σ_{ext} is coming from the differential thermal expansion between the substrate and the film, in our case between the C49 grains and the SiGe matrix. The extrinsic stresses observed in silicides are usually tensile stresses ($\sigma_{ext} > 0$) due to the large mismatch between thermal expansion coefficients: $\sigma_{ext} = \frac{E}{1-\nu} \cdot \Delta\alpha \cdot \Delta T$, where E and ν are Young's modulus and Poisson's ratio of the film, respectively, $\Delta\alpha$ the difference in the linear thermal expansion coefficients between film and substrate (in our case between C49 grains and $\text{Si}_{1-x}\text{Ge}_x$ matrix) and ΔT

the temperature change from T_a to room temperature. To determine $\alpha_{Zr(Si_{1-x}Ge_x)_2}$ and $\alpha_{Si_{1-x}Ge_x}$, we have used a unique linear dependence of the coefficients as a function of Ge-content. This assumption gives us $\frac{\alpha_{ZrSi_2}}{\alpha_{Si}} = \frac{\alpha_{ZrGe_2}}{\alpha_{Ge}} = \frac{\alpha_{Zr(Si_{1-x}Ge_x)_2}}{\alpha_{Si_{1-x}Ge_x}} = 2.96$, where $\alpha_{Si} = 3 \cdot 10^{-6}$ /K and $\alpha_{Ge} = 5.75 \cdot 10^{-6}$ /K. The α_{ZrSi_2} value is obtained by averaging the three expansion coefficients associated to the crystal directions of the unit cell: $\alpha_{ZrSi_2} = 8.88 \cdot 10^{-6}$ /K [31]. Finally, the calculation applied to the C49 film ($x=0.71$) annealed at 815°C gives $\sigma_{ext} = 0.6$ GPa. However, the observation of a compressive stress at room temperature implies that the film is only partially relaxed and that, before cooling, the intrinsic stress is compressive. It has to be noted here that both annealing (RTA) and cooling are extremely rapid. As a consequence, the microstructure is almost quenched. The intrinsic stress value can be deduced from σ and σ_{ext} : $\sigma_{int} = \sigma - \sigma_{ext} = -3.2$ GPa.

From the continuous shift of the 215 cm^{-1} Raman line, it is possible to extend the stress discussion to the whole range of Ge composition. As stress is proportional to the Raman shift, itself linearly dependent of the composition, the stress is linearly x dependent. By fitting σ variations as a function of x, we obtain:

$$\begin{aligned}\sigma(x) &= -(3.2 x + 0.3) \text{ GPa} \\ \varepsilon_R(x) &= -(1.041 x + 0.105) \%\end{aligned}$$

So, σ and ε_R vary from -0.3 GPa and -0.11 % ($x=0$) to -3.5 GPa and -1.15 % ($x=1$), respectively. Similarly, the expression of the averaged strain obtained from the d-spacings (d_{060} , d_{131} , d_{002}) is:

$$\varepsilon_{RX}(x) = -(1.231 x - 0.006) \%$$

The linear x dependence of ε_R and ε_{RX} is displayed in Fig. 9. Remarkable results have been obtained in the whole Ge composition range despite approximations we have done. This is in favour of residual stress in the zirconium germanosilicide films rather than a variation in the Ge stoichiometry.

Similar stress values have been reported in silicides such as $MoSi_2$ and WSi_2 (between -1.6 and -1.9 GPa) [32] and in $Si_{1-x}Ge_x$ layers epitaxially grown on Si(100) by ion-beam sputter deposition (-2.2 GPa for $x=0.3$, 300 nm of thickness; 4.1 GPa for $x=0.6$, 800 nm of thickness) [33].

8. Conclusion

X-ray diffraction experiments have been combined with Raman scattering and electron microscopy data to analyse the result of RTA applied to Zr films sputtered on $Si_{1-x}Ge_x$ epilayers.

The initial formation of ZrSiGe is followed by the formation, at higher temperatures, of the unique C49 $Zr(Si_{1-x}Ge_x)_2$ final phase whatever x and the Zr film thickness between 16 and 80 nm. The C49 formation temperature, denoted by T_p , is lowered by the addition of Ge in the structure. Above the critical Ge composition close to $x=0.33$, the film microstructure becomes textured while it was of

powder-type in films with low x values. As long as the annealing temperature is close to T_f , films are continuous and relaxed. If $T > T_f$, films are no longer continuous and grains are embedded in a $\text{Si}_{1-x}\text{Ge}_x$ matrix. X-ray and Raman data obtained from this type of samples can be understood in terms of Ge non-stoichiometry of the germanosilicide films or residual stress. Nevertheless, the lattice parameter change observed as the annealing temperature exceeds T_f would lead to excessive variations of Ge content in the film. For instance, for $x=0.71$, the d-spacing reductions are $\Delta d_{060} = -0.023 \text{ \AA}$ and $\Delta d_{131} = -0.029 \text{ \AA}$ which would correspond to a Ge content close to $y=0.30$. Although slight Ge stoichiometry variation cannot be definitely ruled out, the combined techniques we have used tend to indicate that the major contribution to the lattice parameter change has a residual stress origin. Some simple evaluations of the corresponding compressive stress have been performed from the 215 cm^{-1} line Raman shift amplitude and d-spacing reduction in the range $[-0.3, -3.5 \text{ GPa}]$ for $0 \leq x \leq 1$ which corresponds to a strain in the range $[-0.11, -1.15 \text{ \%}]$. Additionally, it has been demonstrated that stress variations in the germanosilicide films are linearly dependent on Ge composition, thus very easy to use. Finally, the results show that from d-spacing and Raman spectrum evolutions as a function of the annealing temperature, it is possible to evaluate T_f and then, to prevent film damage due to excessive heating.

Acknowledgements

The authors are very grateful to Profs O. Thomas and G. Lucazeau for their careful and critical reading of the paper.

References

1. Z. Wang, D.B. Aldrich, R.J. Nemanich, D.E. Sayers, Electrical and structural properties of zirconium germanosilicide formed by a bilayer solid state reaction of Zr with strained $\text{Si}_{1-x}\text{Ge}_x$ alloys, *J. Appl. Phys.* 82 (1997), 2342-2348.
2. Y. Yasuda, O. Nakatsuka, S. Zaima, Interfacial reactions of Ti/ and Zr/ $\text{Si}_{1-x}\text{Ge}_x$ /Si contacts with rapid thermal annealing, *Thin Solid Films* 373 (2000), 73-78.
3. Z. Wang, D.B. Aldrich, Y.L. Chen, D.E. Sayers, R.J. Nemanich, Silicide formation and stability of Ti/SiGe and Co/SiGe, *Thin Solid Films* 270 (1995), 555-560.
4. V. Aubry, F. Meyer, R. Laval, C. Clerc, P. Warren, D. Dutartre, Effects of rapid thermal annealing on W/ $\text{Si}_{1-x}\text{Ge}_x$ contacts, *Mat. Res. Soc. Symp. Proc.* 320 (1994), 299-304.
5. V. Aubry-Fortuna, O. Chaix-Pluchery, F. Fortuna, C. Hernandez, Y. Campidelli, D. Bensahel, Structural properties and stability of Zr and Ti germanosilicides formed by rapid thermal annealing, *J. Appl. Phys.* 91 (2002), 5468-5473.
6. D.B. Aldrich, H.L. Heck, Y.L. Chen, D.E. Sayers, R.J. Nemanich, Film thickness effects in the Ti- $\text{Si}_{1-x}\text{Ge}_x$ solid phase reaction, *J. Appl. Phys.* 78 (1995), 4958-4965.
7. D.B. Aldrich, F.M. d'Heurle, D.E. Sayers, R.J. Nemanich, Interface stability of $\text{Ti}(\text{Si}_{1-y}\text{Ge}_y)_2$ and $\text{Si}_{1-x}\text{Ge}_x$ alloys, *Mat. Res. Soc. Symp. Proc.* 402 (1996), 21-26.
8. D.B. Aldrich, Y.L. Chen, D.E. Sayers, R.J. Nemanich, Titanium germanosilicide phase formation during the Ti- $\text{Si}_{1-x}\text{Ge}_x$ solid phase reactions, *Mat. Res. Soc. Symp. Proc.* 402 (1996), 405-410.
9. V. Aubry-Fortuna, A. Eyal, O. Chaix-Pluchery, M. Barthula, F. Meyer, Thermal stability and electrical properties of Zr/ $\text{Si}_{1-x-y}\text{Ge}_x\text{C}_y$ contacts after rapid thermal annealing, *Appl. Phys. Lett.* 73 (1998), 1248-1250.
10. V. Aubry-Fortuna, M. Barthula, J.L. Perrossier, F. Meyer, Contacts on $\text{Si}_{1-x-y}\text{Ge}_x\text{C}_y$ alloys: Electrical properties and stability, *J. Vac. Sci. Technol. B* 16 (1998), 1659-1662.
11. V. Aubry-Fortuna, G. Tremblay, F. Meyer, Y. Miron, Y. Roichman, M. Eizenberg, F. Fortuna, U. Hörmann, H. Strunk, Phase formation and strain relaxation during thermal reaction of Zr and Ti with strained $\text{Si}_{1-x-y}\text{Ge}_x\text{C}_y$ epilayers, *J. Appl. Phys.* 88, 1418 (2000).
12. L.F. Mattheiss, J.C. Hensel, Electronic structure of TiSi_2 , *Phys. Rev. B* 39 (1989), 7754-7759.
13. M. Ianuzzi, L. Miglio, M. Celino, Structural and thermoelastic properties of crystalline and amorphous TiSi_2 phases by tight-binding molecular dynamics, *Phys. Rev. B* 61 (2000), 14405-14413.
14. W.G. Fateley, N.T. McDewitt, F.F. Bentley, Infrared and Raman selection rules for lattice vibrations: The correlation method, *Appl. Spectrosc.* 25 (1971), 155-173.
15. S. Bodnar, J.L. Regolini, Growth of ternary alloy $\text{Si}_{1-x-y}\text{Ge}_x\text{C}_y$ by rapid thermal chemical vapor deposition, *J. Vac. Sci. Technol. A* 13 (1995), 2336-2340.

16. P. Warren, J. Mi, F. Overney, M. Dutoit, Thermal stability of Si/Si_{1-x-y}Ge_xC_y/Si heterostructures grown by rapid thermal chemical vapor deposition, *J. Crystal Growth* 157 (1995), 414-419.
17. J. Mi, P. Warren, P. Letourneau, M. Judelewicz, M. Gailhanou, M. Dutoit, C. Dubois, J.C. Dupuy, High quality Si_{1-x-y}Ge_xC_y epitaxial layers grown on (100) Si by rapid thermal chemical vapor deposition, *Appl. Phys. Lett.* 67 (1995), 259-261.
18. C. Hernandez, Ph.D. thesis, Development and Module Integration of polycrystalline and relaxed monocrystalline layers of SiGe alloys for advanced CMOS, Bipolar and alternative Technologies, Université d'Orléans, september 1999.
19. K. Lyutovich, F. Ernst, F. Banhart, I. Silier, M. Konuma in: A. Cullis and J. Hutchison (Eds), *Microscopy of semiconducting materials*. Institute of Physics Conference Series 157, Institute of Physics Publishing, Bristol, 1997, p. 131.
20. J.B. Lai, L.J. Chen, Effects of composition on the formation temperatures and electrical resistivities of C54 titanium germanosilicide in Ti- Si_{1-x}Ge_x systems, *J. Appl. Phys.* 86 (1999), 1340-1345.
21. B. Chenevier, O. Chaix-Pluchery, I. Matko, J.P. Sénateur, R. Madar, F. La Via, In-situ investigations of the metal/silicon reaction in Ti/Si thin films capped with TiN: volumetric analysis of the C49-C54 transformation, *Appl. Phys. Lett.* 79 (2001), 2184-2186.
22. R. Beyers, R. Sinclair, Metastable phase formation in titanium-silicon thin films, *J. Appl. Phys.* 57 (1985), 5240-5245.
23. T.C. Chou, C.Y. Wong, K.N. Tu, Lattice imaging of metastable TiSi₂, *J. Appl. Phys.* 62 (1987), 2275-2279.
24. O. Chaix-Pluchery, G. Lucazeau, Vibrational study of transition metal disilicides MSi₂ (M=Nb, Ta, V, Cr), *J. Raman Spectrosc.* 29 (1998), 159-164.
25. J.D. Eshelby, *Proc. Roy. Soc. A* 241 (1957), 376-396.
26. J.D. Eshelby *Proc. Roy. Soc. A* 252 (1959), 561-569.
27. J.D. Eshelby, *Progress in Solid Mechanics*, vol. 2, I.N. Sneddon and R. Hill (Eds), North Holland, Amsterdam, 1961, pp 89-140.
28. T. Mura, *Micromechanics and Defects in Solids*, Martinus Nijhoff Publishers, The Hague, Netherlands, 1982, pp 151-158.
29. E. Anastassakis, E. Liarokapis, Polycrystalline Si under strain: Elastic and lattice-dynamical considerations, *J. Appl. Phys.* 62 (1987), 3346-3352.
30. J.F. Jongste, O.B. Loopstra, G.C.A.M. Janssen, S. Radelaar, Elastic constants and thermal expansion coefficient of metastable C49 TiSi₂, *J. Appl. Phys.* 73 (1993), 2816-2820.
31. I. Engström, B. Lönnberg, Thermal expansion studies of the group IV-VII transition metal disilicides, *J. Appl. Phys.* 63 (1988), 4476-4484.
32. F.M. d'Heurle, O. Thomas, Stresses during silicide formation: a review, *Defect and Diffusion Forum* 129-130 (1996), 137-150.

33. F. Meyer, M. Eisenberg, R. Beserman, C. Schwebel, C. Pellet, Raman scattering and stress measurements in $\text{Si}_{1-x}\text{Ge}_x$ layers epitaxially grown on Si(100) by ion-beam sputter deposition, J. Appl. Phys. 70 (1991), 4268-4277.

Figure captions

Fig. 1: X-ray diagrams recorded from 16 nm thick $\text{Zr/Si}_{0.67}\text{Ge}_{0.33}$ films as a function of the annealing temperature: (a) as-dep.; (b) 385°C; (c) 575°C; (d) 770°C; (e) 790°C; (f) 810°C. The hkl reflections written under styles underlined, italic and bold in the figure refer to Zr, ZrSiGe and C49 $\text{Zr}(\text{SiGe})_2$, resp. The reflections marked as Si and SiGe are due to multiple diffraction on Si and SiGe substrates as the sample is continuously rotated around the scattering vector (normal to the film).

Fig. 2: d-spacing variation as a function of x ($0 \leq x \leq 1$) for $\text{Zr}(\text{Si}_{1-x}\text{Ge}_x)_2$ (060), (131) and (002) planes. The films have been annealed at T close to T_f (open symbols) and $T > T_f$ (T_a , full symbols). Full lines are representative of the Vegard's law. The d-spacing values have been obtained from ex-situ diffraction data recorded at room temperature.

Fig. 3: Relative intensity variation for the 060, 131, 002 reflections of C49 $\text{Zr}(\text{Si}_{1-x}\text{Ge}_x)_2$ films as a function of x and Zr thickness : a) 16 nm Zr; b) 80 nm Zr. The line intensities have been normalized to the 131 one.

Fig. 4: $\theta/2\theta$ X-ray diffraction pattern (a) and ω -scans (b) of the 060 reflection measured from 16 nm $\text{Zr/Si}_{0.62}\text{Ge}_{0.38}$ films annealed at different temperatures. The ω -scans have been normalized in intensity and position. T_f is close to or slightly lower than 800°C.

Fig. 5: Raman spectra of C49 $\text{Zr}(\text{Si}_{1-x}\text{Ge}_x)_2$ films (16 nm Zr) obtained by annealing at temperatures close to T_f as a function of x ($0 \leq x \leq 1$). The lines observed in any spectrum at and below 140 cm^{-1} are due to air. The lineshifts of the C49 line centered around 215 cm^{-1} and of the $\text{Si}_{1-x}\text{Ge}_x$ line of the alloy layer have been shown by dotted lines.

Fig. 6: Evolution of the $\text{Zr}(\text{Si}_{1-x}\text{Ge}_x)_2$ Raman line positions as a function of x ($0 \leq x \leq 1$). The lines have been numbered from 1 to 9 for clarity.

Fig. 7: Influence of the annealing temperature on the $\text{Zr}(\text{Si}_{1-x}\text{Ge}_x)_2$ film Raman spectra ($0.33 \leq x \leq 0.71$).

Fig. 8: TEM cross-section image of a C49 $\text{Zr}(\text{Si}_{0.29}\text{Ge}_{0.71})_2$ film (16 nm Zr, $T_a = 815^\circ\text{C}$) :
 (a) C49 grains with different relative orientations and grain sizes (25-65 nm). The C49- $\text{Si}_{1-x}\text{Ge}_x$ interface is rough. The $\text{Si}_{1-x}\text{Ge}_x$ capping layer is clearly featured by thin alternating dark and bright area.

- (b) embedding of the C49 grains at the grain sides completed by a $\text{Si}_{1-x}\text{Ge}_x$ capping layer.
(c) higher magnification of the 1-2-3 grains of image (a). The high-resolution clearly shows stacking faults 120° oriented from one grain to the next.

Fig. 9: X-ray diffraction (ϵ_{RX}) and Raman (ϵ_{R}) determination of the strain added in the C49 films by annealing at $T > T_f$ as a function of x . ϵ_{RX} is obtained by averaging strain values determined from 060, 131 and 002 reflections.

Table captions

Table 1: Intensity and HWHM (α ($^\circ$)) of 060 ω -scans of C49 $\text{Zr}(\text{Si}_{1-x}\text{Ge}_x)_2$ films (16 and 80 nm Zr) obtained at $710^\circ\text{C} \leq T \leq 820^\circ\text{C}$ as a function of x ($0 \leq x \leq 1$). T_f is close to 810, 790, 800, 815, 710, 720 $^\circ\text{C}$ for $x=0, 0.33, 0.38, 0.47, 0.71, 1$, respectively. vw is for very weak, w for weak, s for strong and vs for very strong.

Zr film thickness (nm)	x	T (°C)	060 ω -scans intensity and HWHM (α (°))
16	0	810	vw (-)
16	0.33	790, 810	w (1.3°), vw (-)
16	0.38	710□800, 820	s (3°), s (3.2°), w (1.1°)
16	0.47	815, 820	s (3°), w (0.8°)
16	0.71	710, 815	vs (1.25°), w (0.9°)
16	1	720, 780	vs (1.1°), s (1.0°)
80	0	810	vw (-)
80	0.33	800	vw (-)

Table 1

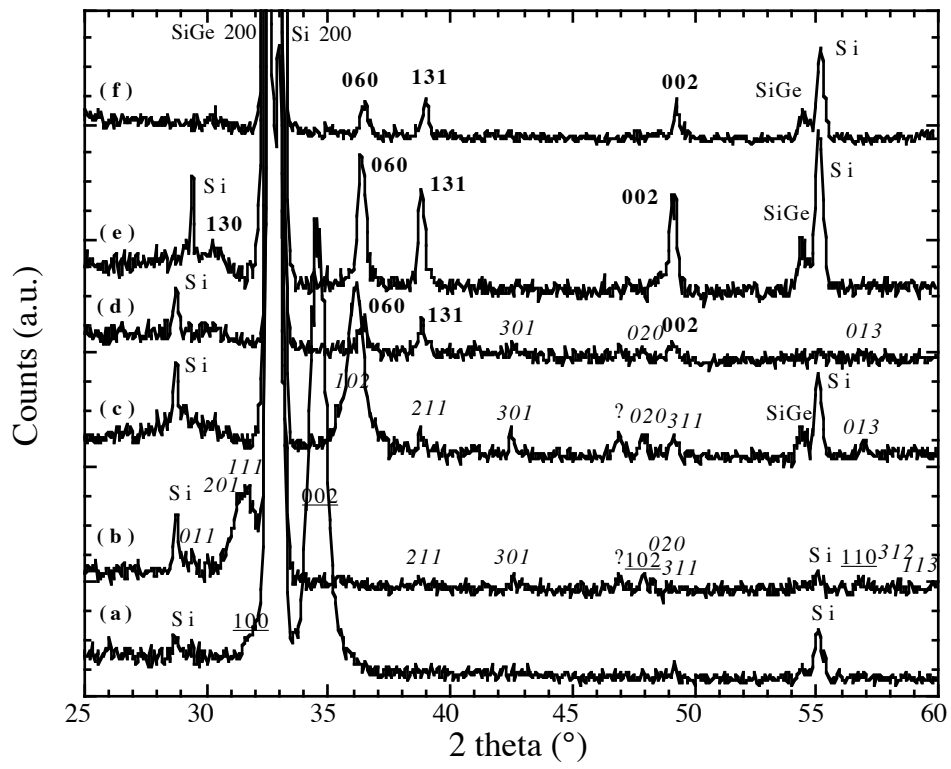
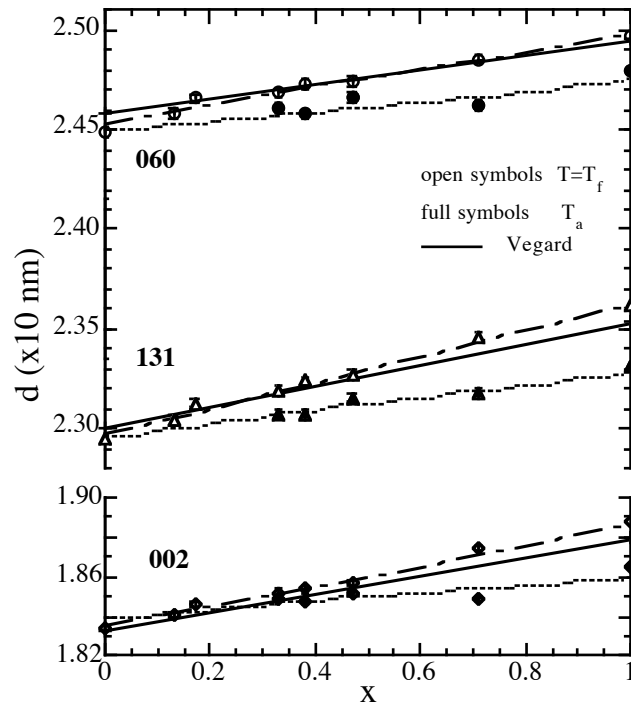
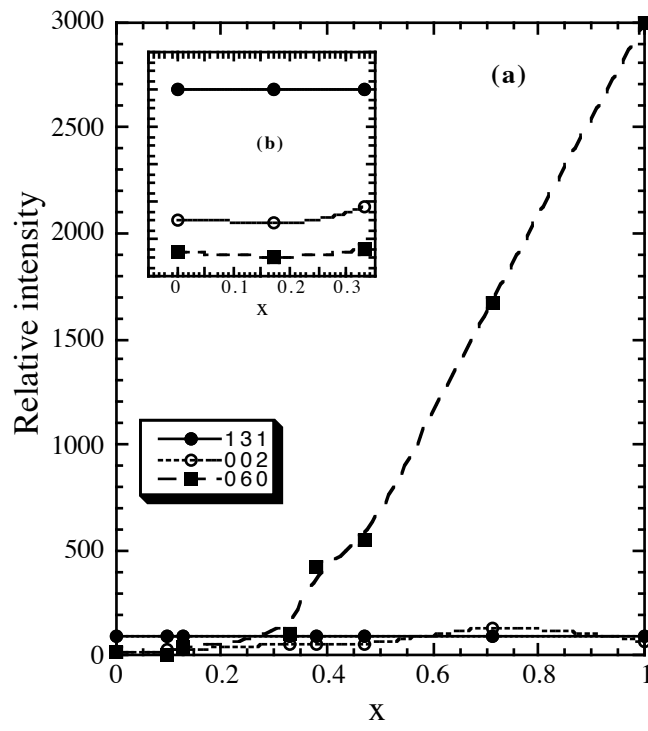
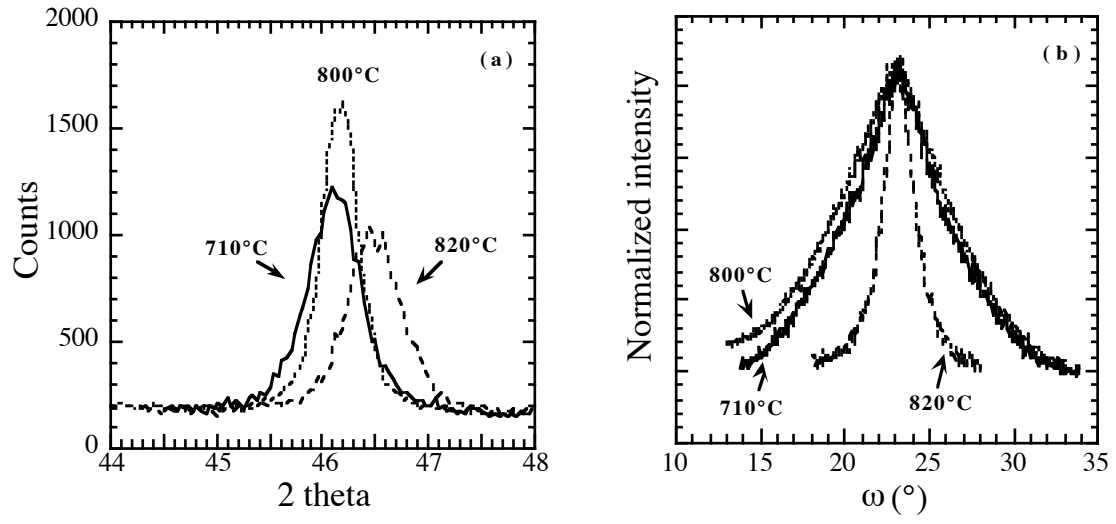
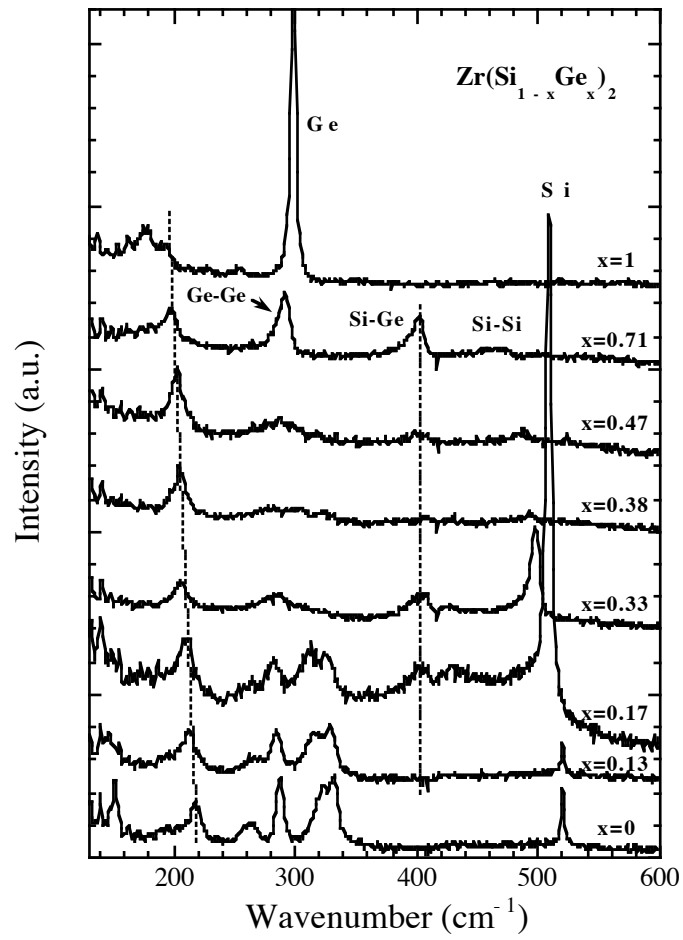


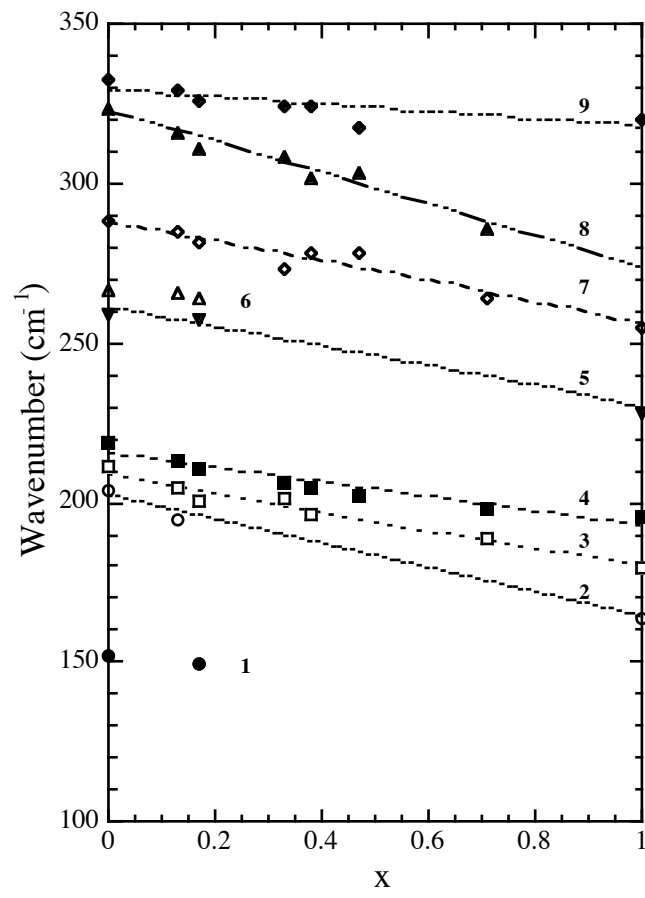
Fig. 1

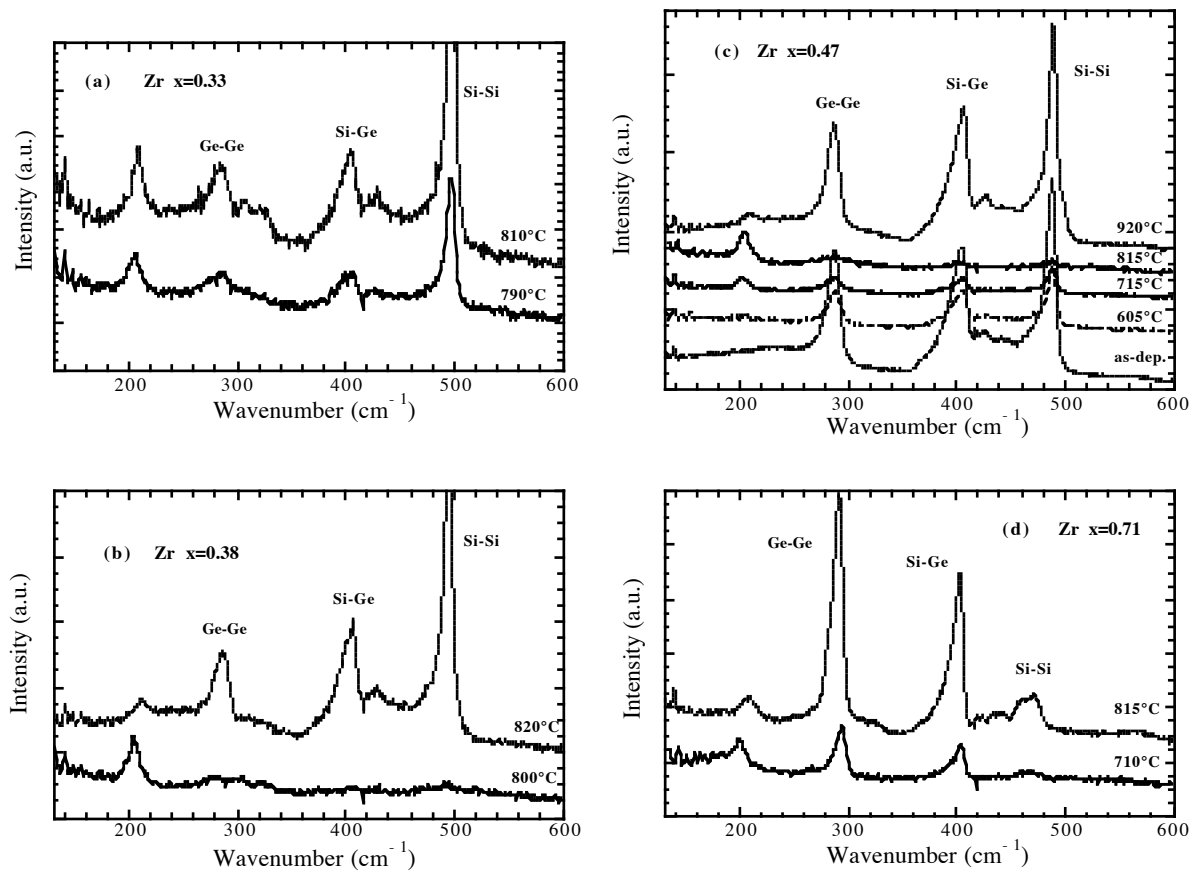
**Fig. 2**

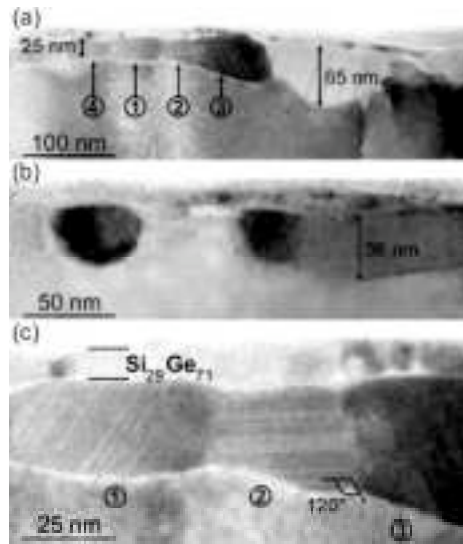
**Fig. 3**

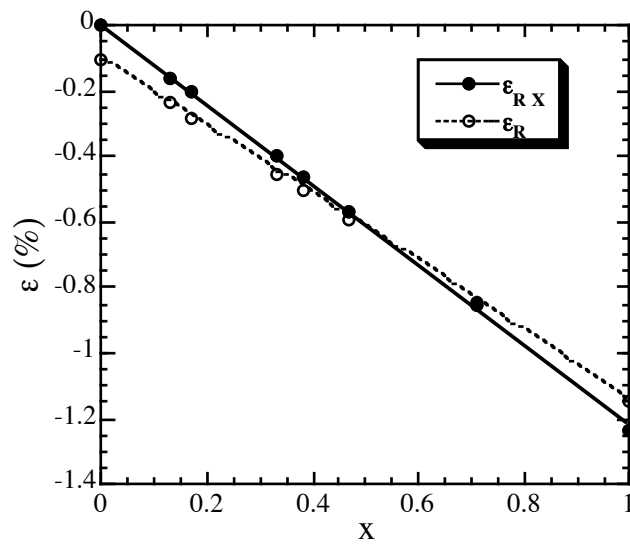
**Fig. 4**

**Fig. 5**

**Fig. 6**

**Fig. 7**

**Fig. 8**

**Fig. 9**